Journal of Research in Science and Engineering (JRSE)
ISSN: 1656-1996 Volume-7, Issue-8, August 2025
DOI: 10.53469/jrse.2025.07(08).06

Classification Model for Lumbar Muscle Fatigue Evaluation Based on Machine Learning

Bo Deng

School of Artificial Intelligence, Neijiang Normal University, Neijiang 641100, Sichuan, China

Abstract: ***In this study, a classification model for lumbar muscle fatigue evaluation was constructed using surface electromyographic (sEMG) signals combined with subjective fatigue assessment scales. Twelve healthy volunteers were selected, and sEMG signals of their lumbar erector spinae muscles were collected; the signals were preprocessed through infinite impulse response (IIR) notch filtering, Butterworth high-pass filtering, and 4-level soft threshold denoising with db4 wavelets, then segmented using a sliding window with a window length of 1000 sampling points and a step size of 200 sampling points, followed by the extraction of 14 features in total (including those from the time domain, frequency domain, time-frequency domain, and nonlinear domain). Feature dimensionality reduction was conducted via recursive feature elimination (RFE) and principal component analysis (PCA); based on 3092 samples categorized into three classes, the performance of six model combinations was compared using 10-fold cross-validation. The results showed that the combination of PCA and random forest (RF) achieved the optimal performance, with an average accuracy of 90.42% and a Kappa coefficient of 0.8056, and both the RF and support vector machine (SVM) models exhibited a recognition rate of over 83% for all three fatigue states. This study demonstrates that the proposed model can realize non-invasive evaluation of lumbar muscle fatigue, thereby providing technical support for related fields.***

Keywords: Surface Electromyographic Signal, Classification Model, Feature, Random Forest**.**

1. Introduction

The global annual incidence of low back pain ranges from 22% to 65%, which can lead to movement disorders and even loss of self-care ability. Chronic lumbar muscle strain is its main inducement, and it is closely related to lumbar muscle fatigue caused by the static and repetitive work of modern people. Therefore, the evaluation of lumbar muscle fatigue has become a key issue to be solved urgently in the fields of medicine and public health [1-3]. Muscle fatigue is divided into central and peripheral types: the former is caused by abnormal neural regulation, while the latter is associated with lactic acid accumulation. The mechanisms involve energy metabolism imbalance, nerve damage, etc. Due to differences in individuals and muscle groups, there is currently no universal evaluation standard [4-5].

Existing evaluations include two categories: subjective and objective. Subjective evaluation is represented by the RPE scale proposed by Swedish scientist Brog, which allows subjects to feedback their fatigue feelings through a score range of 1-20 (1 point corresponds to “very easy” and 20 points corresponds to “extremely strenuous”), and the results are highly correlated with physiological and biochemical indicators. In objective evaluation, surface electromyographic signals (sEMG) are widely used due to their non-invasive and real-time advantages [6-10]. Currently, high-performance electromyographic devices such as Trigno™ and Sessantaquattro have promoted sEMG research [11-13]. Most existing studies focus on the changes in lumbar sEMG features, but there are relatively few lumbar fatigue models based on sEMG [14-16].

In the field of machine learning, algorithms such as KELM and SVM have achieved an accuracy of 64%-94.3% in muscle fatigue classification, providing a basis for model construction [17-20]. In summary, this paper intends to construct a lumbar muscle fatigue evaluation model by combining lumbar muscle sEMG signals with RPE, and carry out relevant research and exploration.

2. Method

2.1 Data Preprocessing

2.1.1 Denoising preprocessing

Data collected by the lumbar surface electromyographic (sEMG) acquisition system contains a large amount of noise, including baseline noise, power-line interference, and other types of noise. Baseline noise is induced by tiny movements caused by muscle contraction and friction between electrodes and skin; the frequency of such motion artifacts is less than 20 Hz. If not filtered out, it will cause signal baseline drift.

In this study, the data were first processed to remove power-line interference using a 50 Hz notch filter designed with an infinite impulse response (IIR) digital filter. Subsequently, a 20 Hz high-pass filter designed with a Butterworth filter was applied for denoising. Among them, the relational expressions between amplitude and frequency of the IIR digital filter and the Butterworth high-pass filter are shown in Equations (1) and (2), respectively:

$$H(s) = \frac{s^2 - \omega_0^2}{s^2 + sQ\omega_0 + \omega_0^2} \tag{1}$$

In the above formula, let the center frequency of the notch filter be the mass factor, which is a complex frequency domain variable.

$$H(s) = \frac{1}{\sqrt{1 + (\frac{s}{\omega_c})^{2n}}} \tag{2}$$

In the above formula, is the complex frequency domain variable, is the cutoff frequency, and represents the order of the filter.

2.1.2 Wavelet soft threshold denoising

Compared with traditional filters, wavelet threshold denoising has stronger time-frequency locality and adaptability: it can retain the features of surface electromyographic (sEMG) signals without additional phase delay, and can adjust adaptively according to frequency components, thus being applied to sEMG denoising [21-22]. Its principle is as follows: perform wavelet transform (WT) on the noisy signal, regard wavelet coefficients with large magnitudes as signal components and those with small magnitudes as noise components, select a threshold to set the noise coefficients to zero, and then reconstruct the signal.

After the signal is transformed by wavelet basis functions, frequency domain information under different frequency and time scales can be obtained, and this transform can highlight the local features of the signal. Different wavelet basis functions correspond to different time-frequency resolutions, which have a significant impact on signal decomposition results. Therefore, in practical applications, selection should be based on signal characteristics and requirements. Common wavelet bases include Daubechies, Haar, Symlets, and Coiflets wavelets. Through denoising experiments on sEMG signals, this study finally selected the db4 wavelet basis from the Daubechies wavelet family, and used this wavelet basis to perform 4-level decomposition on sEMG signals with 10,000 sampling points, as shown in Figure 1.

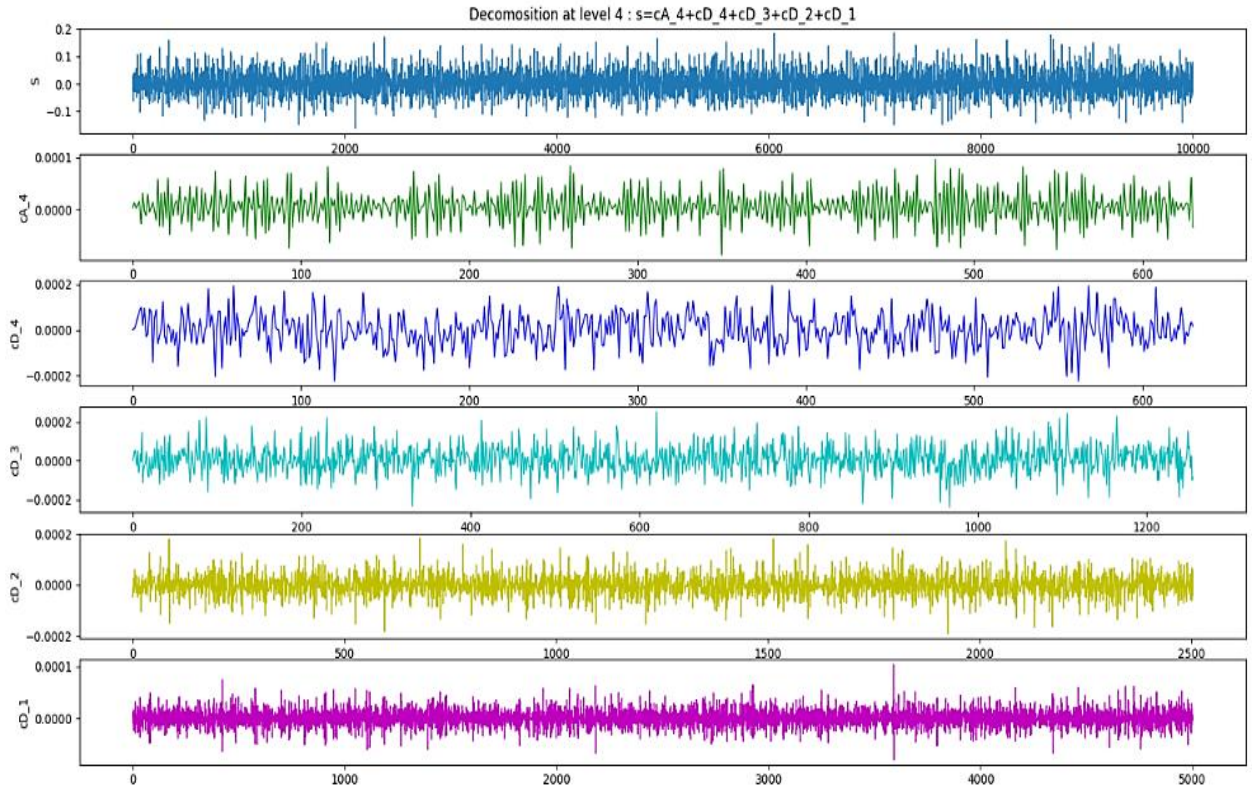

Figures 1: Schematic diagram of 4-layer wavelet decomposition

2.1.3 Data cutting

When this study uses surface electromyographic (sEMG) signals to characterize muscle fatigue, it is necessary to perform data segmentation on the collected signals. Since sEMG signals are acquired as time series, and the signal features and information vary across different time periods, the signals need to be divided into segments according to time windows to extract features and analyze muscle conditions at different stages. Considering that muscle fatigue is a progressive process, the sliding window method in fixed-length segmentation is adopted for signal cutting to avoid signal loss and distortion [23]. The specific sliding window segmentation scheme is shown in Figure 2.

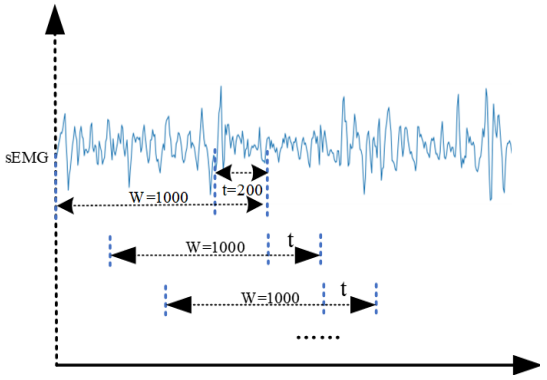

Figures 2: Schematic diagram of sliding window cutting

The window length is 1000 sampling points, the step size is 200 sampling points, and there are 800 overlapping sampling points between two adjacent Windows. If there are X data points, the calculation formula for the number of samples N obtained through segmentation is shown in (3):

$$N = (X - 800)/200 + 1 \quad (3)$$

2.2 Multi-feature Extraction of Surface Electromyographic Signals

2.2.1 Time-domain characteristics

The time-domain features of surface electromyographic (sEMG) signals can directly characterize the changes in muscle status during the fatigue process. In this study, 6

time-domain statistical features were extracted for analysis [24]. The first is integrated electromyography (iEMG), which can reflect the number of motor units involved and their discharge status, and its value is positively correlated with muscle contraction. The second is root mean square (RMS), which can describe the average variation characteristics of sEMG signals over a period of time. The third is average cubic magnitude (ACM), which is commonly used as an indicator to evaluate the degree of muscle fatigue and contraction intensity. The fourth is mean absolute value (MAV), obtained by taking the absolute value of the amplitude of each sampling point in the sEMG signal and then calculating the average. The fifth is variance (VAR), which reflects the degree of dispersion of sEMG signal amplitudes. The sixth is zero-crossing rate (ZCR), referring to the number of times the signal alternates between positive and negative and passes through the zero point. The calculation of all the above features is based on the time series of sEMG signals and their lengths.

2.2.2 Frequency domain characteristics

During muscle fatigue, the function of the neuromuscular junction weakens, leading to a decrease in muscle contraction speed. Consequently, the frequency of surface electromyographic (sEMG) signals gradually decreases, accompanied by spectral leftward shift. In this study, 3 commonly used frequency-domain features were extracted for analysis [25]. The first is median frequency (MF), which refers to the frequency median of muscle electrical activity within a certain period. It represents the middle frequency value of a sorted sEMG signal segment and is used to evaluate the degree of muscle fatigue and muscle function. The second is mean power frequency (MPF), defined as the weighted average of the frequency distribution of sEMG signals over a specific time period. The third is spectral moment (SM); in this study, the second-order spectral moment was adopted to analyze the spectral characteristics of sEMG signals. The calculation of all the above features is based on the frequency, spectrum, or power spectral density function of sEMG signals, as well as the frequency range.

2.2.3 Time-frequency domain characteristics

Compared with traditional time-domain and frequency-domain analysis methods, wavelet analysis can provide more refined frequency-domain analysis results. It can extract more features in different frequency bands, thereby enabling a more comprehensive understanding of the characteristics of muscle activity. The sampling rate of the acquisition system used in this study is 1 kHz; according to the Nyquist sampling theorem, the frequency band range available for wavelet decomposition is 0–500 Hz. In this study, the Daubechies4 (db4) wavelet basis was used to decompose the sEMG signals of lumbar muscles during the fatigue process, with a decomposition level of 4. After discrete wavelet transform (DWT) decomposition, statistical energy feature values were extracted from each subband. by calculating the energy of each subband, this study found that the energy of surface electromyographic signals in each frequency band of cD4, cD3, cD2, and cD1 showed a relatively obvious increasing trend with the deepening of the fatigue process. Therefore, the energy values of these 4 subbands were selected as feature values.

2.2.4 Nonlinear characteristics

Approximate entropy (ApEn) is a nonlinear dynamic parameter used to measure the regularity and unpredictability of time series. Expressed as a non-negative number, it characterizes the complexity of the sequence: a larger value indicates a more complex sequence and a higher probability of new information appearing, which can reflect the irregularity of the sequence. During analysis, parameters such as time delay and similarity criterion must first be selected; then, the similarity of samples is calculated to estimate the approximate entropy, thereby evaluating the irregularity and complexity of the signal. In muscle fatigue analysis, the state of muscles can be evaluated by comparing the approximate entropy values of different time periods.

The calculation of approximate entropy requires the following steps: first, determine parameters such as the signal sequence and pattern dimension; second, construct multi-dimensional vectors; third, calculate the ratio of the number of approximate vectors to the total number of vectors; fourth, increase the dimension and repeat the above steps; finally, obtain the approximate entropy. In this study, the pattern dimension is usually set to 2, and the similarity measurement value is related to the standard deviation of the sequence.

2.3 Feature Dimensionality Reduction

2.3.1 Recursive feature elimination

Feature selection is a crucial task in machine learning. It selects representative and predictive features from a large number of features, thereby improving the learning and generalization capabilities of the model. Feature selection methods are categorized into three types: filter methods, embedded methods, and wrapper methods. The wrapper method selects the optimal feature subset by constructing feature subsets, training models, and evaluating model performance [26].

In this study, the recursive feature elimination (RFE) algorithm—belonging to the wrapper methods—was adopted. This algorithm gradually removes features that have little impact on the model's classification performance to improve accuracy and generalization ability. In each iteration, the features with the least impact are eliminated based on the model's performance, and this cycle is repeated until the required number of features remains.

2.3.2 Principal Component Analysis

In this study, Principal Component Analysis (PCA) was additionally selected as a feature dimensionality reduction method. It significantly reduces the consumption of model training time and storage space without decreasing the classification accuracy.

The main idea of the PCA dimensionality reduction method is to identify n comprehensive variables to replace the original m variables. These comprehensive variables are intended to represent the information of the original variables as much as

possible, while being mutually uncorrelated with each other.

The implementation of PCA involves the following steps: first, decentralize the data to obtain a zero-mean data matrix; second, calculate the covariance matrix of this data matrix; third, perform eigenvalue decomposition on the covariance matrix to obtain new eigenvalues and their corresponding eigenvectors. The new eigenvalues are sorted in descending order according to their contribution rates to form a projection matrix. Assuming there are m principal components, the calculation formula for the contribution rate of the i-th principal component is shown in Equation (4).

$$\eta_i = \frac{\lambda_i}{\sum_{h=1}^{m} \lambda_h} \quad (4)$$

3. Result

3.1 DATA

The experimental subjects consisted of 12 volunteers (6 males and 6 females). Meanwhile, the subjects were required to meet the following criteria: no low back pain caused by any reason or limited limb movement within the past six months, no history of neuromusculoskeletal diseases, and all of them were right-handed.

Before the official start of the experiment, all subjects were informed of and familiarized with the experimental process, content, and objectives. Meanwhile, they were required to sign the informed consent form in advance. The subjects were also requested not to engage in strenuous exercise, consume alcohol, stay up late, or participate in similar activities within 48 hours before the experiment.

3.2 Experimental Results

3.2.1 Feature analysis

Since there is instability in the collected signals at the beginning and end of the formal lumbar muscle fatigue induction experiment, the data of the first 10 seconds before the experiment and the last 5 seconds after the experiment were removed in this study. Figure 3 below shows the complete surface electromyographic (sEMG) data of the left and right lumbar erector spinae muscles of a typical subject during the entire fatigue process.

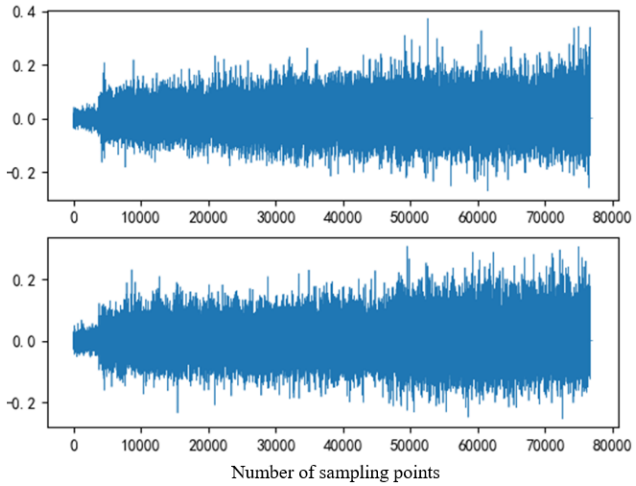

Figures 3: The original data graph of a certain subject

It can be seen from Figure 3 that the amplitude of the surface electromyographic (sEMG) signal of the left erector spinae muscle of this subject is slightly larger than that of the right erector spinae muscle. During the fatigue process, the sEMG signal amplitudes of the left and right lumbar erector spinae muscles of the subject both showed an increasing trend with the passage of time. Although there are differences in the changes of their sEMG amplitudes, the change trends are consistent, which also indirectly proves the feasibility of the fatigue induction experiment.

3.2.2 Feature dimension reduction analysis

In this study, the Recursive Feature Elimination (RFE) algorithm was used for feature selection, and five-fold cross-validation was applied to verify the prediction accuracy of feature subsets, which served as the basis for feature subset selection. The recursive feature elimination plots based on three classifiers—Linear Discriminant Analysis (LDA), Support Vector Machine (SVM), and Random Forest (RF)—are shown in Figure 4 below.

During RFE based on Random Forest (RF), it was observed that as the feature subset dimension increased to 5, the prediction accuracy of the RF classification model continued to rise. Subsequently, as the feature subset dimension further increased, the accuracy fluctuated. It was not until the feature subset was selected as a 17-dimensional one that the five-fold cross-validation prediction accuracy of RF reached the highest. At this point, this study selected the 17-dimensional feature subset as the feature set for the RF classifier.

Similarly, during RFE based on Support Vector Machine (SVM), when the feature subset dimension was 12, the average prediction accuracy was the highest; accordingly, this study selected the 12-dimensional feature subset as the feature set for the SVM classifier. For RFE based on Linear Discriminant Analysis (LDA), a 7-dimensional feature subset was selected as the feature set for the LDA classifier.

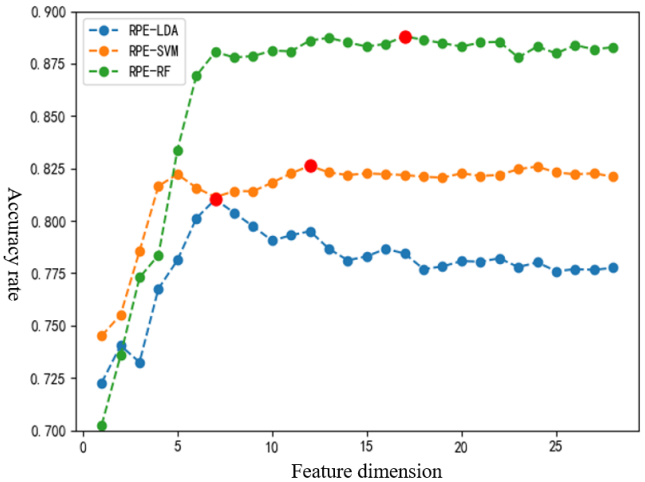

Figures 4: Feature recursive elimination graphs of three classifiers

3.2.3 Analysis of Classification Results

After 3,092 valid samples belonging to three categories in this study were randomly shuffled, ten-fold cross-validation (which makes full use of data and improves the reliability of model evaluation) was used to evaluate six models

(combining 3 classifiers and 2 dimensionality reduction methods). The results showed that: the six models exhibited different accuracy rates for the three fatigue states (see Figure 5), and the recognition rate of the fatigue transition state was generally low (possibly due to subjects' difficulty in accurately reporting their fatigue status); the accuracy rates for all three states exceeded 80%, with Random Forest (RF) and Support Vector Machine (SVM) (both exceeding 83%) outperforming Linear Discriminant Analysis (LDA). For the same classifier, the impact of Recursive Feature Elimination (RFE) and PCA dimensionality reduction showed little difference, but RFE had higher computational cost, making PCA more optimal. Among the six models, LDA performed poorly while RF performed the best; among them, the PCA+RF combination achieved an average accuracy rate of 90.42% and a Kappa value of 0.8056. Therefore, this study selected the combination of PCA and Random Forest for identifying lumbar muscle fatigue states.

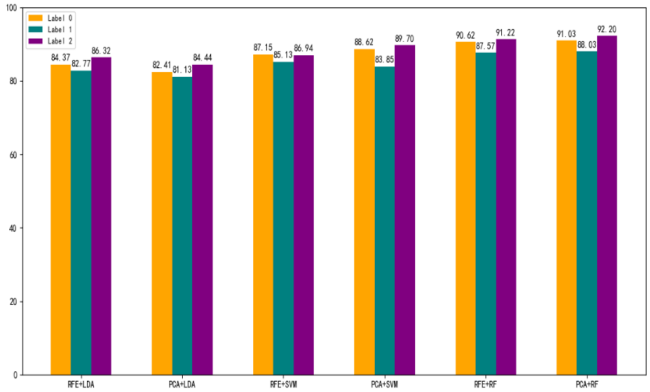

Figures 5: Accuracy result graphs of different fatigue states

Conclude

To address the issue of lumbar muscle fatigue evaluation, this study used surface electromyographic (sEMG) signals of the lumbar erector spinae muscles from 12 healthy volunteers as data and incorporated the Rating of Perceived Exertion (RPE) scale to construct a model; after denoising procedures—including Infinite Impulse Response (IIR) notch filtering, Butterworth high-pass filtering, and 4-level soft threshold denoising with db4 wavelet—data segmentation was performed using a sliding window with a window length of 1000 sampling points and a step size of 200 sampling points, and subsequently 14 multi-dimensional features were extracted. Through dimensionality reduction via Recursive Feature Elimination (RFE) and Principal Component Analysis (PCA), a total of 3,092 samples categorized into three classes were used to compare 6 model combinations via ten-fold cross-validation, with the PCA+Random Forest (RF) combination exhibiting the optimal performance (achieving an average accuracy of 90.42% and a Kappa value of 0.8056) and the recognition rates of RF and Support Vector Machine (SVM) exceeding 83%. The experiment showed that the sEMG amplitudes of the left and right erector spinae muscles increased with the progression of fatigue, while the recognition rate of the fatigue transition state was relatively low, and this model can provide non-invasive evaluation support for related fields, though further optimization is required in subsequent studies.

References

[1] Chenot J F, Greitemann B, Kladny B, et al. Non-specific low back pain[J]. Deutsches Ärzteblatt International, 2017, 114(51-52): 883.

[2] Mosabbir A. Mechanisms behind the development of chronic low back pain and its neurodegenerative features[J]. Life, 2022, 13(1): 84.

[3] Sun W, Zhang H, Lv C, et al. Comparative efficacy of 12 non-drug interventions on non-specific chronic low back pain in nurses: a systematic review and network meta-analysis[J]. Journal of Back and Musculoskeletal Rehabilitation, 2021, 34(4): 499-510.

[4] Boccia G, Dardanello D, Zoppirolli C, et al. Central and peripheral fatigue in knee and elbow extensor muscles after a long‐distance cross‐country ski race[J]. Scandinavian journal of medicine & science in sports, 2017, 27(9): 945-955.

[5] Tornero-Aguilera J F, Jimenez-Morcillo J, Rubio-Zarapuz A, et al. Central and peripheral fatigue in physical exercise explained: A narrative review[J]. International Journal of Environmental Research and Public Health, 2022, 19(7): 1-16.

[6] Li P, Yang X, Yin G, et al. Skeletal muscle fatigue state evaluation with ultrasound image entropy[J]. Ultrasonic Imaging, 2020, 42(6): 235-244.

[7] Lee K H, Zhang Y Z, Kim H, et al. Muscle fatigue sensor based on Ti3C2Tx MXene hydrogel[J]. Small Methods, 2021, 5(12): 1-9.

[8] Brausch L, Hewener H, Lukowicz P. Classifying Muscle States with One-Dimensional Radio-Frequency Signals from Single Element Ultrasound Transducers[J]. Sensors, 2022, 22(7): 2789.

[9] Ding W, You T, Gona P N, et al. Validity and reliability of a Chinese rating of perceived exertion scale in young Mandarin speaking adults[J]. Sports Medicine and Health Science, 2020, 2(3): 153-158.

[10] Toro S F, Santos-Cuadros S, Olmeda E, et al. Is the use of a low-cost sEMG sensor valid to measure muscle fatigue? [J]. Sensors, 2019, 19(14): 3204.

[11] Moore E, Fuller J T, Buckley J D, et al. Impact of cold-water immersion compared with passive recovery following a single bout of strenuous exercise on athletic performance in physically active participants: a systematic review with meta-analysis and meta-regression [J]. Sports Medicine, 2022, 52(7): 1667-1688.

[12] Fisher S R, Rigby J H, Mettler J A, et al. The effectiveness of photobiomodulation therapy versus cryotherapy for skeletal muscle recovery: a critically appraised topic[J]. Journal of sport rehabilitation, 2019, 28(5): 526-531.

[13] SO R C. Effect of transcutaneous electrical acupoint stimulation on fatigue recovery of the quadriceps[J]. Eur J Appl Physiol, 2007, 100: 693-700.

[14] Pizzolato S, Tagliapietra L, Cognolato M, et al. Comparison of six electromyography acquisition setups on hand movement classification tasks[J]. PloS one, 2017, 12(10): e0186132.

[15] Mao S, Li J, Guo A, et al. An active multielectrode array for collecting surface electromyogram signals using a-IGZO TFT technology on polyimide substrate[J]. IEEE Transactions on Electron Devices, 2020, 67(4): 1613-1618.

[16] Devries H A, Tichy M W, Housh T J, et al. A method for estimating physical working capacity at the fatigue threshold (PWCFT)[J]. Ergonomics, 1987, 30(8): 1195-1204.
[17] Hua A, Bai J, Hao Z, et al. Linear spectrum and non-linear complexity features of lumbar muscle surface electromyography between people with and without non-specific chronic low back pain during Biering-Sorensen test[J]. Journal of Electromyography and Kinesiology, 2023, 69 (4): 102742.
[18] Karvekar S, Abdollahi M, Rashedi E. Smartphone-based human fatigue level detection using machine learning approaches[J]. Ergonomics, 2021, 64(5): 600-612.
[19] Krishnamani D B, PA K, Swaminathan R. Variational mode decomposition based differentiation of fatigue conditions in muscles using surface electromyography signals[J]. IET Signal Processing, 2020, 14(10): 745-753.
[20] Mulla M, Sepulveda F. A comparison of sEMG and MMG signal classification for automated muscle fatigue detection[J]. International Journal of Biomedical Engineering and Technology, 2019, 30(3): 277-293.
[21] BAŞPINAR U, ŞENYÜREK V Y, DOĞAN B, et al. A comparative study of denoising sEMG signals[J]. Turkish Journal of Electrical Engineering and Computer Sciences, 2015, 23(4): 931-944.
[22] Li C, Cao D, Yuan Y. Research on improved wavelet denoising method for sEMG signal[C]//2019 Chinese Automation Congress (CAC). IEEE, 2019: 5221-5225.
[23] Farfán F D, Politti J C, Felice C J. Evaluation of EMG processing techniques using information theory[J]. Biomedical engineering online, 2010, 9: 1-18.
[24] Yousif H A, Zakaria A, Rahim N A, et al. Assessment of muscles fatigue based on surface EMG signals using machine learning and statistical approaches: a review[C] //IOP conference series: materials science and engineering. IOP Publishing, 2019, 705(1): 012010.
[25] Chowdhury S K, Nimbarte A D, Jaridi M, et al. Discrete wavelet transform analysis of surface electromyography for the fatigue assessment of neck and shoulder muscles[J]. Journal of Electromyography and Kinesiology, 2013, 23(5): 995-1003.
[26] Rouhani H, Fathabadi A, Baartman J. A wrapper feature selection approach for efficient modelling of gully erosion susceptibility mapping[J]. Progress in Physical Geography: Earth and Environment, 2021, 45(4): 580-599.